J Mater Sci (2011) 46:5991–5999
DOI 10.1007/s10853-011-5560-2

Shock behaviour of a phenolic resin

David C. Wood · Paul J. Hazell · Gareth J. Appleby-Thomas · Nick R. Barnes

Received: 25 February 2011 / Accepted: 11 April 2011 / Published online: 22 April 2011

Abstract Phenolic resins are used in many aspects of everyday life, e.g. as the matrix material for carbon fibre laminates used in the aerospace industry. Consequently, detailed knowledge of this material, especially while under shock loading, is extremely useful for the design of components that could be subjected to impact during their lifespan. The shock Hugoniot equations of state for phenolic resin (Durite SC-1008), with initial density of 1.18 g cm^{-3} have been determined using the plate-impact technique with in situ manganin stress gauges. The Hugoniot equation in the shock velocity–particle velocity plane was found to be non-linear in nature with the following equation: $U_S = 2.14 + 3.79u_p - 1.68u_p^2$. Further, the Hugoniot in the pressure–volume plane was observed to largely follow the hydrostatic curve. Lateral gauge measurements were also obtained. An ANSYS Autodyn^{TM} 2D model was used to investigate the lateral stress behaviour of the SC-1008. A comparison of the Hugoniot elastic limit calculated from the shear strength and measured sound speeds gave reasonable agreement with a value of 0.66 ± 0.35 GPa obtained.

Introduction

Phenolic resins have a wide range of applications which include, but are not exclusive to, electrical insulation, kitchen utensils [1] and use in heat-shields for the aerospace industry [2]. Phenolic resins are used in such applications due to their resistance to abrasion and dimensional stability over a range of operating temperatures, with this latter property due to the fact that phenolic resins are thermosetting plastics. The use of phenolic resins in the aerospace industry and the consequent possibility of impact damage, reinforces the requirement for knowledge of shock propagation in such materials.

Many methods can be used for generating shock in materials including contact explosives [3], laser ablation [4] as well as plate impact technique [5] employed here. Five key parameters are needed to understand the behaviour of shocked materials. These are shock velocity U_S, particle velocity u_p, density ρ, pressure P and internal energy E. Usefully, only two parameters are needed to fully define a shock. The Rankine–Hugoniot equations [6], based on the principles of conservation of energy, mass, and momentum then allow the other three parameters to be calculated. The parameters measured in this study were U_S and σ_x, with u_p found using the impedance matching technique [6], while density was calculated from the Rankine–Hugoniot equations. This allowed the Hugoniots in the U_S–u_p and P–V planes to be ascertained.

Hugoniot relationships in the U_S–u_p plane are generally linear in nature following Eq. 1, where c_0 is the intercept at zero particle velocity and S is the resultant slope of the Hugoniot. However, non-linear relationships do occur [7, 8]. In such cases, a second order quadratic equation, of the form shown in Eq. 2, may be employed. Such non-linear equations of state have also been used in computational simulations of polymers, e.g. Ref. [9].

$$U_S = c_0 + Su_p \quad (1)$$

$$U_S = c_0 + S_1u_p + S_2u_p^2 \quad (2)$$

The hydrostatic pressure P_H due to a shock in a material is given by Eq. 3 which can be written in the form of

D. C. Wood (✉) · P. J. Hazell · G. J. Appleby-Thomas
Cranfield University, Cranfield Defence and Security, Shrivenham, Swindon SN6 8LA, UK
e-mail: d.wood@cranfield.ac.uk

N. R. Barnes
AWE, Aldermaston, Reading, Berkshire RG7 4PR, UK

Eq. (4) for the pressure-volume plane, where ρ_0 is the initial density with v and v_o being the volume at a given pressure and initial volume, respectively. The Hugoniot in the U_S–u_p plane is used to calculate the value of P_H.

$$P_H = \rho_0 U_S u_p \tag{3}$$

$$P_H = \rho_0 U_S^2 \left(1 - \frac{v}{v_0}\right) \tag{4}$$

In addition, the hydrostatic (P_H) and deviatoric (τ) elements of stress are linked by Eq. 5. This equation implies that if the longitudinal stress equals the hydrostatic pressure then there is little to no strength effect in the material.

$$\sigma_x = P_H + \frac{4}{3}\tau \tag{5}$$

With polymers the depth of knowledge with regards to the shock response varies greatly, from materials that are well defined, e.g. polymethylmethacrylate (PMMA) [7, 8], to materials that have been little studied. Further, it has been shown that different samples of the same polymer can have different shock Hugoniot profiles due to slightly different compositions or manufacturing processes. Such behaviour is clearly exhibited by the abundant scatter of data noticed by Barker and Hollenbach in PMMA [7].

Carter and Marsh [8] studied the shock response of 20 polymers. For all polymeric materials studied, they consistently found a discrepancy between the zero pressure intercept of the U_S–u_p curve and the ultrasonically measured sound speeds. They attributed this phenomena to the forces between adjacent polymer chains being orders of magnitude lower than the forces along the backbone of the polymer, making initial compression two-dimensional in nature. Such behaviour was shown to lead to non-linearity in the U_S–u_p plane. The subsequent linear behaviour of the Hugoniot at elevated particle velocities was thought to represent the three-dimensional compressive behaviour. It was also found that a phase change occurred in many of the polymers investigated in the 20–30 GPa range.

In the literature, there is limited knowledge on the shock behaviour of phenolic resins with most studies concerned with phenolic resins as part of a composite system. Carter and Marsh, however, did include the phenolic resin Durite HR 300-Borden in their investigations.

The dynamic response of epoxy-resins has been more extensively studied [8, 10–12]. Munson and May [10] investigated the effect of different hardeners which resulted in different structures along with different levels of cross linking. They found that in the U_S–u_p plane a single equation could explain the behaviour. In the pressure–volume plane there was no noticeable discrepancy between the epoxies with different hardeners over the investigated range which reached values of 2 GPa.

Another epoxy resin RTM-6, used as the matrix component in aerospace-grade carbon fibre composites, was studied by Hazell et al. [11]. Its dynamic behaviour was found to be comparable to that of other epoxy resins. Furthermore deviation from the hydrostatic pressure was seen in RTM-6 above 4 GPa. In other work, Appleby-Thomas et al. [12] investigated the lateral stress behaviour of RTM-6. The Hugoniot elastic limit and dynamic yield strength for RTM-6 was found to be comparable to other epoxy resins.

Millett et al. [13] investigated the shock behaviour of a composite which included different ratios of alumina particulates in an epoxy resin. As alumina particulates were used the sample was considered to be isotropic in nature allowing for a simplified analysis. It was found that by increasing the ratio of alumina particles in the epoxy, the sample material started to behave similarly to a metal or ceramic.

In this work, the dynamic shock behaviour of a phenolic resin SC-1008 was investigated using manganin stress gauges. These gauges measure the longitudinal and lateral stresses induced in the samples. From this data U_S–u_p and P–V Hugoniot relationships were derived.

Experimental techniques

The experimental method employed for this investigation was the plate impact technique. This involved using a ø 50 mm, 5 m barrel, single-stage gas gun [5] which accelerates a flyer plate into a target material, with all the surfaces perpendicular to the direction of impact machined flat and parallel to ±5 μm. The experimental setup for the gun, also showing a typical target configuration, is shown in Fig. 1. The flyer and cover plate were made of the same material, usually Aluminium (Dural) or Copper, employed due to their well-characterised nature, e.g. [14]. Further, the target is attached to a sacrificial barrel extension. Taken together these measures ensured that any misalignment on impact was consistently less than 1.5 mrad [15].

Vishay Micro-measurements manganin stress gauges of types LM-SS-125CH-048 and J2M-SS-580SF-025 were employed for longitudinal and lateral shots, respectively. Longitudinal gauges measure the longitudinal stress exerted on the material whereas the lateral gauges give a stress which is dependent on the strength of the sample [16]. These gauges were used due to their stable behaviour over a wide range of temperatures. As stress is exerted on the manganin gauge element, a change in resistance of the gauge occurs. Using a calibration technique detailed by Rosenberg et al. [17] for longitudinal gauges and Rosenberg et al. [18, 19] and Millett et al. [20] for lateral gauges, this allows calculation of in-material stress. The longitudinal gauges were

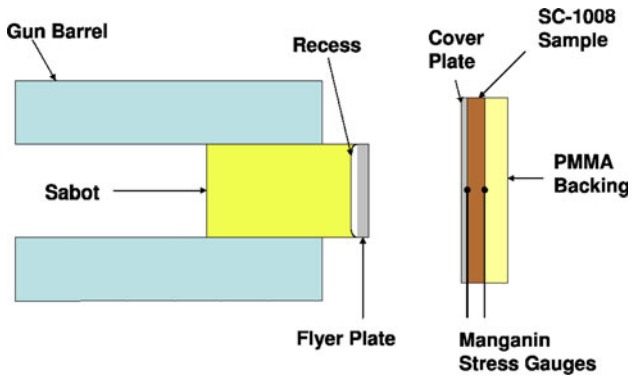

Fig. 1 General experiment setup

protected by layers of 25 μm thick Mylar®, which also insulated them from the cover plate. However, the lateral gauges were already encapsulated in their as-manufactured state and therefore did not require additional Mylar® protection. All components were glued together using slow curing Locite 0151 HYSOL® Epoxi-Patch® adhesive. Finally, before component assembly accurate sample thickness measurements were made using a micrometer. Typical gauge/sample arrangements are shown in Fig. 2.

Computational modeling

A commercially available hydrocode (ANSYS Autodyn™) was employed to aid interpretation of recorded lateral stress profiles. Two-dimensionally axially symmetric models employing an Euler mesh with cell sizes of 100 μm were constructed. Material models consisted of equations of state in conjunction with a Drucker–Prager strength model [21]. The initial Autodyn™ model setup is shown in Fig. 3.

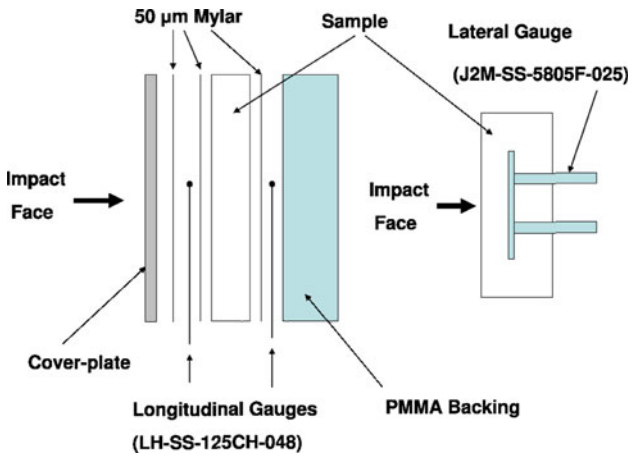

Fig. 2 Typical gauge/sample layouts: longitudinal on the *left* and lateral on the *right*

Material

The phenolic resin investigated was Durite SC-1008. This was supplied by Lockheed Martin (UK) in 30 mm diameter spheres. The samples were sectioned with material taken from the centre of the sphere, thereby giving an approximate thickness of 4 mm while keeping the diameter at ~30 mm. Due to the small size of the SC-1008 phenolic resin target, a containment ring was used to ensure the one-dimensionality of the shock through the sample for the duration of the experiment. The containment ring arrangement with inserted resin (bonded in place with an epoxy resin) is shown schematically in Fig. 3.

The density of the SC-1008 phenolic resin was measured using a Micrometrics AccuPyc 1330 gas pycnometer. In addition longitudinal (c_L) and shear (c_S) sound velocities were measured ultrasonically using a 1 MHz quartz transducer with a Panametrics 5077PR pulse receiver in the pulse–echo configuration. Key elastic material properties for SC-1008 are shown in Table 1, with the bulk sound speed c_B calculated using Eq. 6. The shear modulus (G) of the material was calculated using Eq. 7.

$$c_B = \sqrt{c_L^2 - \frac{4}{3}c_S^2} \tag{6}$$

$$G = \rho_0 c_S^2 \tag{7}$$

Results and discussion

The experimental data for longitudinal and lateral shots is presented in Table 2. For the lateral shot data, σ_x was estimated from the known impact conditions. A typical longitudinal trace is shown in Fig. 4.

The rear gauge trace in Fig. 4 has been calibrated according to Eq. 8 [12], based on known impact

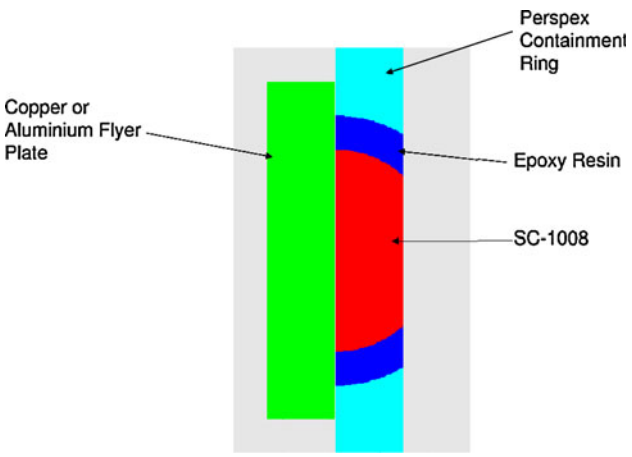

Fig. 3 Setup of the Autodyn™ model

Table 1 Key elastic material properties of SC-1008

ρ_0 (g cm^{-3})	c_L (mm μs^{-1})	c_S (mm μs^{-1})	c_B (mm μs^{-1})	v	G (GPa)
1.18	2.67	1.38	2.14	0.36	2.24

conditions, to calculate the true stress in the SC-1008 rather than the backing PMMA (see Fig. 2). Both the front and re-calibrated rear surface longitudinal gauge traces exhibit very similar profiles. Following an initial rise (typically ~50 ns duration, compared to ~100 ns for the lateral traces shown later in Fig. 7) observed on shock arrival, an overshoot in stress combined with ringing results, with the frequency of ringing being 18 MHz suggesting an electrical effect. Following the initial overshoot in stress, a constant plateau known as the Hugoniot stress, is observed in both cases. The good agreement between the front and impedance matched rear Hugoniot stresses appears to be confirmation that the experiment was truly one-dimensional; validating the encapsulation technique employed. The Hugoniot stress is maintained until release waves from the rear of the flyer arrive ending the one-dimensional nature of the shot. An apparent multi-stage release than occurs on both gauges, before eventual gauge failure.

$$\sigma_{\text{Sample}} = \frac{1}{2}\frac{Z_{\text{Sample}} + Z_{\text{Backing}}}{Z_{\text{Backing}}}\sigma_{\text{Rear gauge}} \quad (8)$$

Experimental results are shown graphically in the shock velocity-particle velocity plane in Fig. 5 and the pressure-volume plane in Fig. 6, along with literature data for other broadly similar polymeric materials. The RTM-6 data was obtained from Hazell et al. [11], with the alternative phenolic data from Carter and Marsh [8].

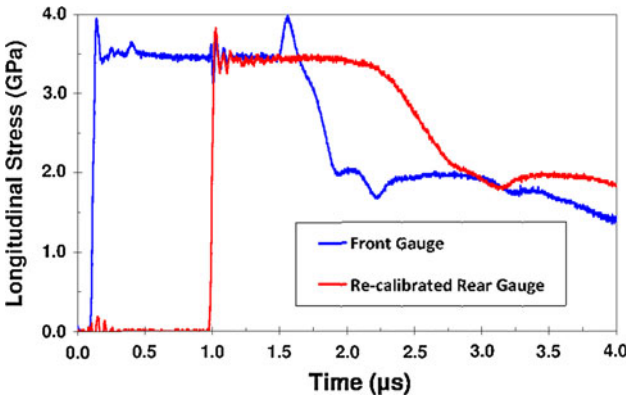

Fig. 4 Typical longitudinal gauge traces for SC-1008; impacted by a 5 mm Copper flyer at 960 ms^{-1}

As seen in Fig. 5, the SC-1008 U_S-u_p Hugoniot appears to have a non-linear nature within the particle-velocity regime investigated. Essentially, a polynomial curve of the type detailed in Eq. 2 produced the optimum fit to the experimental data. In this case, the polynomial coefficients for the best-fit were: $c_0 = 2.14$ mm μs^{-1}, $S_1 = 3.79$, and $S_2 = -1.68$ μs mm^{-1}. Such a non-linear response has been observed previously in other polymeric materials particularly at low particle velocities/pressures. For example, PMMA [7], polycarbonate replacement resin [22], and various epoxy resins [8], have all exhibited such behaviour. As discussed previously, such a non-linear response at low particle velocities has been attributed to the substantial difference in magnitude between backbone and inter-chain forces [8]. Essentially, weaker inter-chain forces are overcome during the initial stages of compression before stronger backbone covalent bonds can be affected. This then results in non-linear behaviour at low particle

Table 2 Experimental results obtained using longitudinal and lateral gauges

Velocity (ms^{-1})	Flyer thickness/ material (mm)	U_S (mm μs^{-1})	u_p (mm μs^{-1})	v (cm^{-3} g^{-1})	σ_x /P (GPa)	σ_y (GPa)	Yield strength (GPa)
145	5 Cu	–	–	0.81	0.36 (estimated)	0.19	0.17
200	10 Al	2.69	0.16	0.80	0.51	–	–
320	10 Al	–	–	0.78	0.92 (estimated)	0.55	0.37
350	10 Al	3.19	0.27	0.78	0.97	–	–
485	10 Al	3.11	0.38	0.75	1.39	–	–
500	10 Al	–	–	0.75	1.59 (estimated)	1.01	0.58
600	10 Cu	3.77	0.53	0.73	2.31	–	–
670	10 Cu	–	–	0.71	2.68 (estimated)	1.96	0.72
						–	
810	10 Al	3.87	0.62	0.71	2.90		–
865	10 Cu	–	–	0.69	3.65 (estimated)	2.61	1.04
						–	
960	5 Al	3.88	0.73	0.69	3.46		–
970	5 Cu	4.26	0.85	0.68	4.65	–	–

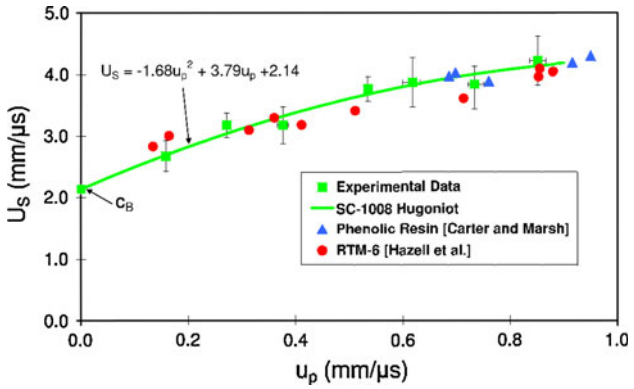

Fig. 5 Hugoniot of SC-1008 in the U_S–u_p plane with comparable resins [8, 11]

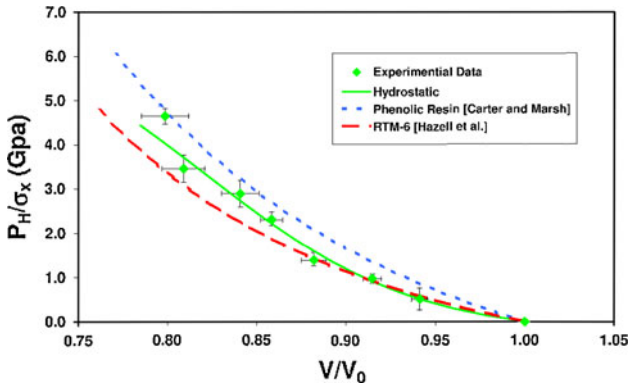

Fig. 6 Hugoniot of SC-1008 in the pressure-volume plane with comparable resins [8, 11]

velocities, before a more conventional linear U_S–u_p response is established as compression continues.

It is interesting to note that the lowest particle-velocity portion of the U_S–u_p phenolic resin data found by Carter and Marsh [8], included in Fig. 5, is in very good agreement with the highest u_p data ($u_p > 0.6$ mm μs^{-1}) measured for SC-1008 here. Given that Carter and Marsh found a linear relationship of the type shown in Eq. 1 for their phenolic resin over the pressure range between 4 and 20 GPa, and in line with the fact that U_S–u_p relationships for epoxy resins are typically very similar independent of the precise resin tested [10, 11], this result suggests a two-stage U_S–u_p behaviour in SC-1008 (and potentially phenolic resins in general). Initially, for u_p below 0.7–1.0 mm μs^{-1} a non-linear polynomial Hugoniot will result, while at elevated impact pressures a linear response will be established. Interestingly, while slightly more linear in nature, there is also good general agreement between the included RTM 6 data from Ref. [11] and that for SC-1008.

In Fig. 6, V/V_0 (the normalised volume attained during the experiment on the abscissa) is plotted against P. The use of V/V_0 allows direct comparisons with different materials. On the P–V/V_0 plot the hydrostat is plotted according to Eq. 3. All of the experimental data with the exception of the highest value lies on the hydrostat. From Eq. 5 this implies that, initially at least, the SC-1008 possesses no strength under shock loading. However, above 4 GPa deviation is seen from the hydrostat implying the material is starting to strengthen behind the shock front. This behaviour is similar to other polymeric materials including polycarbonate [23], polypropylene [24], polystyrene [24] and RTM-6 [11]. Further, the compressibility of the SC-1008 is initially the same as the epoxy resin RTM-6 until ~1 GPa. Above this point, the SC-1008 becomes less compressible compared to RTM-6. In addition, the phenolic resin investigated here is more compressible than the phenolic resin investigated by Carter and Marsh.

Figure 7 shows all of the lateral traces for the shots detailed in Table 2 plotted together with a recentered time base. The traces show an overshoot on the three higher pressure shots likely attributable to an electrical effect within the gauge. The pressure then stabalises to a plateau due to the lateral stress exerted on the material. A ramp-up is seen towards the end of the shot, and this has been computationally shown to be due to shock reflections from the interface between the edge of the SC-1008 sample and the epoxy resin interlayer used in the containment process. Investigation of the source of this re-loading involved a series of Autodyn^{TM} hydrocode models. This was achieved by using the setup explained in the computational modeling section and, for the case detailed here, the impact conditions of a 500 ms^{-1} shot employing a 10 mm aluminium flyer plate. In all cases, a moving point gauge element was inserted 4 mm from the impact face of the sample. In addition, this gauge was also radially offset from the impact axis by 4 mm. The material equations of state used in the Autodyn^{TM} model for aluminium, perspex, and epoxy were obtained from the in-built Autodyn^{TM} library. For the SC-1008 phenolic resin, the experimentally determined polynomial equation of state employing the

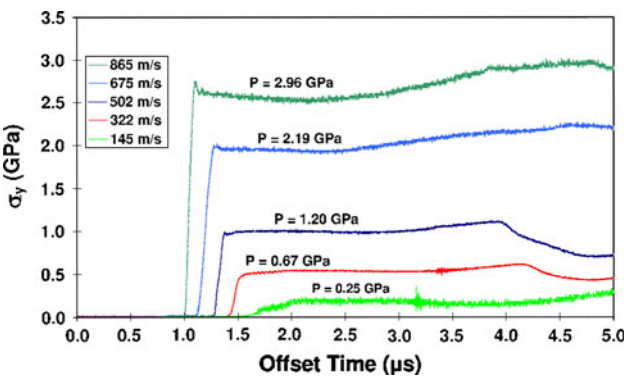

Fig. 7 Lateral gauge traces for SC-1008

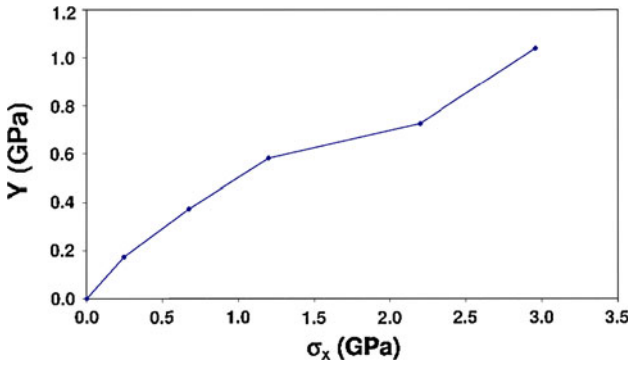

Fig. 8 Pressure-yield surface used in the Drucker–Prager strength model based on experimental measurements of σ_y

calculated values of density, S_1, S_2 and c_0 was used. The inelastic response was accounted for by the Drucker–Prager strength model, that employs a pressure-dependent yield surface [25–27]. Here Eqs. 9 and 10 were used to calculate pressure and yield strength (Y) using the relevant σ_x and σ_y values from Table 2. The resultant yield surface, e.g. the Drucker–Prager strength model is shown in Fig. 8.

$$P_{\text{Average}} = \frac{\sigma_x + 2\sigma_y}{3} \tag{9}$$

$$Y = 2\tau = \sigma_x - \sigma_y \tag{10}$$

Figure 9 shows reasonable agrement between the experimental data and computer simulation in terms of general behaviour, with a discrepancy in lateral stress of about 0.1 GPa. Analysis of the temporal evolution of the sample showed that the increase in gradient occurring at about 1.5 μs after shock arrival was due to the shock reflection occurring at the SC-1008 and epoxy resin interlayer. The timing and overall form of this reflection was seen to be linked to the geometry of the retained SC-1008 resin sample. It is worth noting that the arrival of this shock refection also marked the end of the one-dimensional

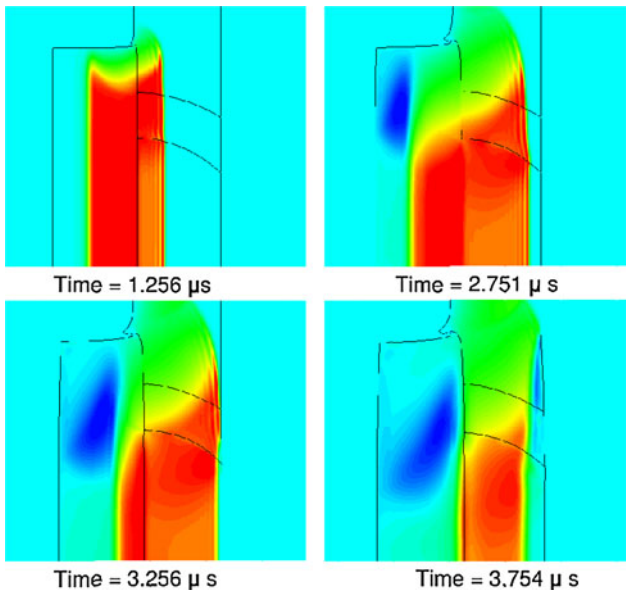

Fig. 10 Behaviour of shock in Autodyn™ model

behaviour in the sample. A sequence of frames showing the evolution of pressure in the model is presented in Fig. 10.

It should be noted that the gauge used in the model was a point element whereas in the experiments the lateral gauge was a 16 mm manganin wire element. Moving the gauge element in the computational model, the position at which 1D behaviour finished could be altered. By moving the gauge closer to the centre of the sample, the ramped behaviour was either delayed or became non-existent. Conversely, moving the gauge closer to the edge of the SC-1008 resin sample resulted in a more rapid loss of one-dimensionality in the gauge response. Due to the nature of the target confinement and geometry this response was not entirely unexpected.

The discrepancy noted above between the computational model and the experimental results in lateral gauges continues over the whole range of investigated shock pressures. In Fig. 11, the ratio of experimentally measured lateral

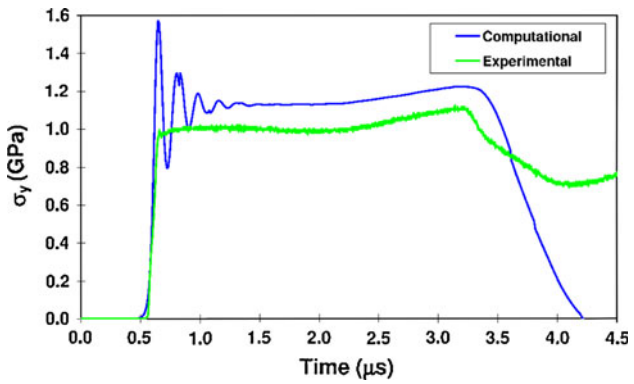

Fig. 9 Comparison of computational model and experimental lateral stresses (a 10 mm Aluminium flyer impacting at 508 ms^{-1})

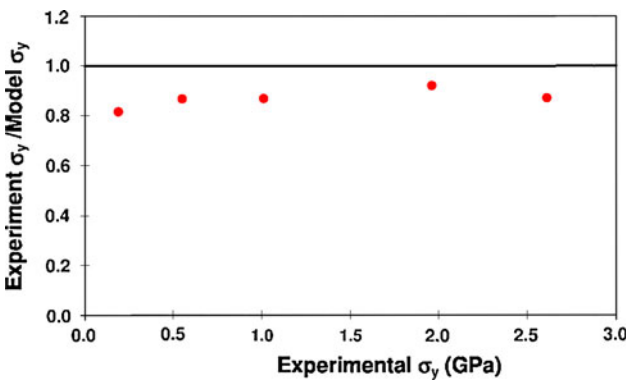

Fig. 11 Discrepancy between computational and experimental lateral stress

stresses to computational results is plotted against measured lateral stress. If the Autodyn™ model matches up to the experimental results, a situation which should occur due to the experimental results being used in the Drucker–Prager strength model, this ratio should be close to unity. However, as shown in Fig. 11, this is clearly not the case. Instead the ratio is consistently around 0.8 to 0.9—approximately 10–20% lower than might be expected. Further, this discrepancy is observed to vary in a non-linear manner with measured lateral stress—an effect linked to the non-linear nature of the shear strength data employed in the Drucker–Prager strength model (as shown in Fig. 8).

By comparing the yield strength of the material to an elastic prediction given by Eq. 11, the Hugoniot elastic limit can be ascertained. The Hugoniot elastic limit is the point at which the elastic–plastic transition occurs. Below the Hugoniot elastic limit, the material behaves elastically and above this point it is plastic in nature. This approach is shown graphically in Fig. 12. From this, the Hugoniot elastic limit was found to be 0.66 ± 0.35 GPa. As indicated in Fig. 12, this relatively wide error simply arises due to the larger experimental errors encountered at elevated impact pressures. In addition, an approximate value for the Hugoniot elastic limit was found using Eq. 12. The value of c_L detailed in Table 1 was used in Eq. 2 to obtain the maximum possible particle velocity in the elastic regime (e.g. the u_p intercept of c_L with the U_S–u_p Hugoniot shown in Fig. 5). This value, $u_H \sim 0.1$ mm μs^{-1}, gave a maximum value for the HEL of 0.3 GPa. This value, while low in comparison to the intersect shown in Fig. 12, lies just on the edge of the calculated error band. Given the aforementioned issues with calculating an HEL from the intercept of the predicted elastic and measured plastic shear strength curves in Fig. 12, the fact that these values are of similar orders of magnitude suggests that the average HEL of 0.66 ± 0.35 GPa from Fig. 12 is a reasonable approximation.

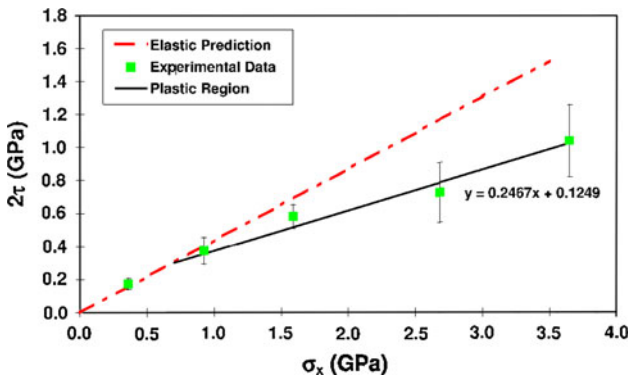

Fig. 12 Graph used for calculation of Hugoniot elastic limit

$$2\tau = \frac{1-2\nu}{1-\nu}\sigma_x \tag{11}$$

$$\sigma_{HEL} = c_L \rho_0 u_H \tag{12}$$

Further, this reasonable agreement between the Hugoniot elastic limit values calculated (1) from the shear strength-impact stress plot in Fig. 12, and (2) directly from the ultrasonically measured elastic sound speed, appears to confirm the validity of the use of measured lateral stress values to calculate shear strengths. However, it should be noted that there is currently a degree of contention within the shock physics community with regards to the interpretation of such data. In particular, Winter and Harris [28] and Winter et al. [29] have recently highlighted the fact that there is often a difference between near and far field lateral stress response in materials due to the inherently intrusive nature of the encapsulated lateral manganin stress gauges employed. These authors employed both experiment and simulation to interrogate shock propagation through (a) a so-called matrix material, and (b) a matrix material with an embedded fluid layer—considered analogous to an encapsulated lateral gauge. The presence of the fluid layer was found to modify the nature of the shock front. In particular, behaviour on shock arrival and behind the shock front was strongly influenced by the relative fluid layer/matrix shock velocities. Slower shock velocity in the central fluid layer led to a ramp to a peak followed by a subsequent decrease in stress with time; whereas a faster fluid shock velocity was shown to result in a relatively slow initial ramp-up, with longitudinal stress subsequently increasing behind. In both cases, comparison of experiment and simulation appeared to suggest that the gauge response tended towards the true material (rather than encapsulating matrix) stress with time. These findings suggest that care should be taken in the interpretation of lateral gauge traces. However, here—as shown in Fig. 7—before the re-loading due to the target confinement highlighted in Fig. 9, there is only a relatively minor gradient in stress behind the shock. Consequently, lateral stresses measured by the epoxy-encapsulated lateral gauges are likely reasonably representative of far-field SC-1008 stresses. Further, in line with recent work by Appleby-Thomas et al. [30], it is likely that given the similarity in impedance—and therefore shock velocity—between polymeric materials, minimal shock dispersion would have occurred in the epoxy lateral gauge interlayer. Nevertheless, the small resultant errors in measured lateral stress caused by these issues are likely to, at least partially, explain the discrepancy between the shear-strength and elastic sound-speed based predicted material elastic limits. Rosenberg and Partom [31] made the case that the HEL of polymers could be calculated using a pressure-dependent yield surface which would alter Eq. 11. This would then result in different values for the elastic

prediction used for calculating the HEL. However, other authors have successfully used the model employed here, hence we feel justified in using the approach presented in this article.

In addition to the questions over the use of embedded lateral manganin stress gauges outlined above, the results presented here also draw attention to a further potential issue. Essentially, under the one-dimensional impact conditions of a plate impact experiment, because strain will be confined along the impact axis (defined as the x-axis), σ_y and σ_z will be equal. Consequently, by definition, the hydrostatic pressure (P) will be given by Eq. 9. For a hydrodynamic material shear strength, τ, will tend to zero. In such a situation Eq. 5 reduces to $\sigma_x = P_H$. Substituting this result into Eq. 9 (taking $P_H = P_{Average}$), it can be shown that in a strength-less material σ_x should be equal to σ_y. However, as can be seen in Table 2, this is clearly not the case here; in fact, when calculated the ratio σ_y/σ_x is observed to trend to about 0.8 at higher impact stresses, rather than trending to unity as would be expected. At lower stresses this is likely due to inaccuracies inherent in the employment of manganin stress gauges in such stress regimes [6]. However, at higher stresses this behaviour suggests a degree of material strength. This is despite the fact that SC-1008 has been shown to behave hydrodynamically (e.g. Fig. 6) at impact stresses ≤ 4.0 GPa. Similar behaviour, with the ratio of σ_y/σ_x tending to < 1, despite observed hydrodynamic behaviour over the impact regime of interest, is observed elsewhere in the literature, e.g. Refs. [12, 23, 32–35]. Consequently, such a response may be indicative of a systematic calibration issue with lateral gauges in this class of materials. However, in order for such a conclusion to be reached a careful study of lateral gauge response in a variety of materials would be required - something outside the scope of this article. However it is notable that there has been a wide adoption within the literature of the lateral gauge-based approach to estimation of material shear strength (albeit by a relatively limited number of authors), e.g. Refs. [12, 23, 32–38]. In addition, as mentioned previously, in this study, this approach has led to reasonable agreement with the HEL value calculated from the measured elastic sound speed. Consequently, the decision has been taken here to utilise the resultant calculated HEL. Nevertheless, the potential for inaccuracy due to gauge calibration issues is acknowledged.

Conclusion

The shock loading response of a phenolic resin SC-1008 has been investigated using the flyer plate impact technique. A non-linear Hugoniot in the U_S–u_p plane was found, following the equation $U_S = 2.49 + 3.79u_p - 1.68u_p^2$. In the P–V/V_0 plane, the experimental results closely followed the hydrostatic pressure suggesting minimal strengthening under shock loading. It was also found that the phenolic resin SC-1008 behaved in a similar manner to other polymeric materials that are used in comparable applications. An Autodyn™ model was used to help visualise the behaviour seen in the lateral stress traces. This behaviour was found to be due to the geometric nature of the resin sample. The pressure calculated from the model was shown to be close to the experimental data, albeit with a consistent discrepancy of $\sim 10\%$. Finally, a Hugoniot elastic limit was calculated from both measured shear strength and ultrasonic sound speed data, with good agreement found leading to a value of 0.66 ± 0.35 GPa being assumed.

Acknowledgements The authors would like to acknowledge the support of the Institute of Shock Physics and AWE as well as Lockheed-Martin Insys for supplying the samples used for experimentation. We also wish to thank Mr. Andrew Roberts for technical help with the experiments. British Crown Copyright MOD/2011.

References

1. Cowie JMG (1991) Polymers: chemistry and physics of modern materials. Blackie, Glasgow, p 17
2. Burrell RH, Barnes NK, Keightley PT, Millett JCF, Bourne NK (2009) In: Americian Physical Society, 16th APS conference, poster presentation
3. Fujiwara S (1992) In: Sawaoka AB (ed) Shock compression technology and material science. KTK Scientific Publisher, Tokyo, p 7
4. Boustie M, Berthe L, de Resseguier T, Arrigoni M (2008) In: 1st International symposium on laser ultrasonics: science, technology and applications
5. Bourne NK (2003) Meas Sci Technol 14:273
6. Meyers MA (1994) Dynamic behavior of materials. Wiley-Interscience Publication, New York, p 116
7. Barker LM, Hollenbach RE (1970) J Appl Phys 41:4208
8. Carter WJ, Marsh SP (1995) Hugoniot equation of state of polymers. Report LA-13006-MS. Los Alamos National Laboratory, Los Alamos
9. Porter D, Gould PJ (2009) Int J Solids Struct 46:1981
10. Munson DE, May RP (1972) J Appl Phys 43:962
11. Hazell PJ, Stennett C, Cooper G (2008) Polym Comp 29:1106
12. Appleby-Thomas G, Hazell P, Stennett C (2009) J Mater Sci 44:6187. doi:10.1007/s10853-009-3859-z
13. Millett JCF, Bourne NK, Deas D (2005) J Phys D 38:930
14. Marsh SP (1980) LASL shock hugoniot data. University of California Press, California
15. Stennett C, Cooper GA, Hazell PJ, Appleby-Thomas GJ (2009) In: Proceedings of the American Physical Society Topical Group on shock compression of condensed matter, 2009, American Institute of Physics, Melville, p 267
16. Volger TJ, Chhabildasa LC (2006) Int J Imp Eng 33:812
17. Rosenberg Z, Yaziv D, Partom Y (1980) J Appl Phys 51:3702
18. Rosenberg Z, Brar NS (1995) J Appl Phys 77:1443
19. Rosenberg Z, Partom Y (1985) Lateral stress measurement in shock-loaded targets with transverse piezoresistance gauges. J Appl Phys 58:3072
20. Millett JCF, Bourne NK, Rosenberg Z (1996) J Phys D 29:2466

21. Van Den Berg P, De Borst R, Hutink H (1996) J Numer Anal Methods Geomech 20:865
22. Appleby-Thomas GJ, Hazell PJ, Stennett C, Cooper G, Cleave R (2009) In: DYMAT 2009, 9th International conference on the mechanical and physical behaviour of materials under dynamic loading, vol 2, p 1081
23. Millett J, Bourne N (2006) J Mater Sci 41:1683. doi: 10.1007/s10853-006-3951-6
24. Millett JCF, Bourne NK (2004) J Phys D Appl Phys 37:2901
25. Park SW, Xia Q, Zhou M (2001) Int J Imp Eng 25:887
26. Tham CY (2005) Finite Elem Anal Des 41:1401
27. Ma GW, Hao H, Zhou YX (1998) Comp Geotech 22:283
28. Winter RE, Harris EJ (2003) J Phys D 41:035503
29. Winter RE, Owen GD, Harris EJ (2008) J Phys D 41:202006
30. Appleby-Thomas GJ, Hazell PJ, Wilgeroth JM, Wood DC (2010) J Appl Phys 108:033524
31. Rosenberg Z, Partom Y (1994) J Appl Phys 76:1935
32. Millett JCF, Bourne NK, Barnes NK (2002) J Appl Phys 92:6590
33. Bourne NK, Millett JCF, Goveas SG (2007) J Phys D 40:5714
34. Millett JCF, Bourne NK, Gray III GT, Cooper G (2002) In: Shock compression of condensed matter 2001, 12th APS topical conference, American Institute of Physics, Melville, p 131
35. Millett JCF, Bourne NK, Gray III GT (2004) J Phys D 37:942
36. Pickup IM, Millett JCF, Bourne NK (2004) In: Shock compression of condensed matter 2003, proceedings of the conference of the American Physical Society Topical Group, American Institute of Physics, Melville, p 751
37. Ragford DD (2005) J Appl Phys 98:063504
38. Appleby-Thomas GJ, Hazell PJ (2010) J Appl Phys 107:123508
39. Bourne NK, Millett JCF (2003) Proc R Soc London Ser A 459:597